

Latent representation prediction networks

Hlynur Davið Hlynsson*, Merlin Schüler, Robin Schiewer, Tobias Glasmachers, Laurenz Wiskott Institut für Neuroinformatik, Ruhr-Universität Bochum, D-44801 Bochum, Germany

* hlynur.hlynsson@ini.rub.de

Abstract

Deeply-learned planning methods are often based on learning representations that are optimized for unrelated tasks. For example, they might be trained on reconstructing the environment. These representations are then combined with predictor functions for simulating rollouts to navigate the environment. We find this principle of learning representations unsatisfying and propose to learn them such that they are directly optimized for the task at hand: to be maximally predictable for the predictor function. This results in representations that are by design optimal for the downstream task of planning, where the learned predictor function is used as a forward model.

To this end, we propose a new way of jointly learning this representation along with the prediction function, a system we dub Latent Representation Prediction Network (LARP). The prediction function is used as a forward model for search on a graph in a viewpoint-matching task and the representation learned to maximize predictability is found to outperform a pre-trained representation. Our approach is shown to be more sample-efficient than standard reinforcement learning methods and our learned representation transfers successfully to dissimilar objects.

Introduction

While modern reinforcement learning algorithms reach super-human performance on tasks such as gameplaying, they remain woefully sample inefficient compared to humans. An algorithm that is data [48] or sample-efficient [47] requires only few samples for good performance and the study of sample-efficient control is currently an active research area [5] [44] [46] [49].

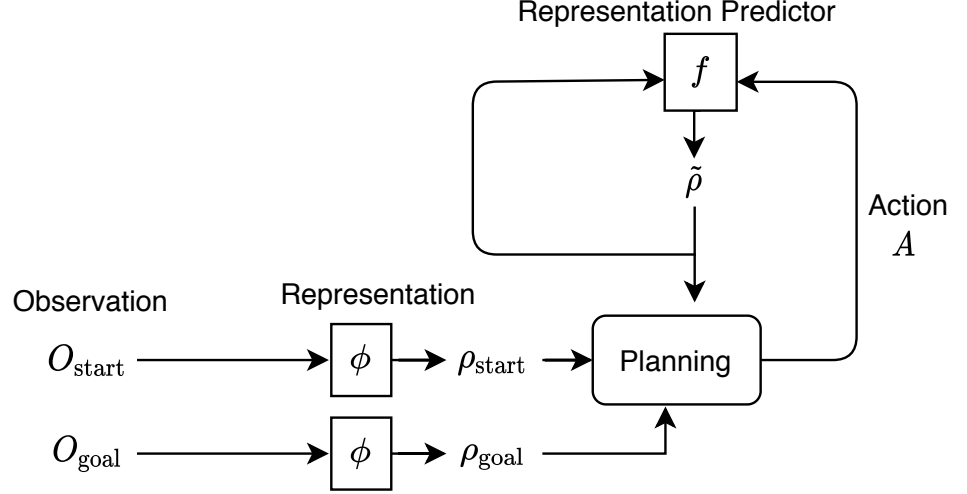
A centrepiece of human cognition is the remarkable ability to create accurate mental models of our environments and perform mental simulations [6]. There has been much recent work on methods that take advantage of compact representations of states for search and exploration [20] [5] [41]. One of the advantages of this approach is that a good representation aids in faster and more accurate planning. This holds in particular when the latent space is of much lower dimensionality than the state space [58].

Many real-world situations can be reduced to partially-observable Markov decision processes (POMDP) [59]. Under this general framework, there are *agents* taking *actions* A changing their environment's *state* S . The information that they have on the states comes from the *observations* O they perceive as not all the details of the state in a POMDP is generally known. How the environment's state S_t at a time step t changes after an action A_t is performed is governed by the transition function $T(S_t, A_t)$. After the action A_t is realized, the system grants the agent a reward R_t , whose value is determined by the reward function $R(S_t, A_t)$. Under the POMDP framework, a mental

model can be interpreted as a suitable latent space representation of the observations coupled with an estimation of the transition function [6].

This paper introduces *Latent Representation Prediction* (LARP) networks, a neural network-based method for learning a domain representation and a POMDP transition function for planning within the learned latent space (Fig. 1). During training, the representation ϕ and the predictor f are learned simultaneously from transitions in a supervised manner. The predictor predicts the most likely resulting future representation given a current representation along with an action.

Fig 1. Conceptual overview of our method. The important components are the representation network ϕ along with the predictor network f . Together, they comprise a LARP network which is utilized by a planning algorithm.



We study three different approaches to avoid the trivial constant representation being learned by the base ϕ , which would result in a maximally predictable – although useless – representation. To avoid this degenerate representation, we (i) design the architecture such that the output is spherized, (ii) regularize with a contrastive loss term, or (iii) include a reconstruction loss term along with an additional decoder module. The predictor is used during downstream planning tasks for navigating a latent space and finding a goal state.

We validate our approach experimentally on a visual environment: a viewpoint-matching task using the NORB data set [1], where the agent is presented with a starting viewpoint of an object and the task is to produce a sequence of actions such that the agent ends up with the goal viewpoint. As the NORB data set is embeddable on a cylinder [2] [3] or a sphere [4], we can visualize the actions as traversing the embedded manifold.

Optimizing control after learning the environment model has the advantage of allowing for learning new reward functions in a fast and sample-efficient manner. Disentangling the reward from the transition function is helpful when learning for multiple or changing reward functions and aids with learning when there is no reward available at all. Thus, it is also good for a sparse or a delayed-reward setting.

Related work

Most of the related work falls into the categories of reinforcement learning, visual planning or representation learning. The primary conceptual shortcoming of other

model-based methods is that the representation is learned by solving an auxiliary task, such as reconstruction, which is not of direct interest for maximizing rewards.

Reinforcement learning

We approximate a Markov decision process’ state transition function so similarities are plentiful in the reinforcement learning literature: many agents perform explicit latent-space planning computations [7] [8] [9] [10] [11] [12] as part of learning and executing policies. Gelada et al. [13] train a reinforcement learning (RL) agent to simultaneously predict rewards as well as future latent states. Our work is distinct from these as we are not assuming a reward signal and are dependent on fewer known POMDP parameters during training.

Vision, memory, and controller modules are combined for learning a model of the world before learning a decision model in Ha and Schmidhuber’s World Models [15]. A predictive model is trained in an unsupervised manner, permitting the agent to learn policies completely within its learned latent space representation of the environment. The main difference is that they first approximate the state distribution using a variational autoencoder, producing the encoded latent space. In contrast, our representation is learned such that they are maximally predictable for the predictor network.

Similar to our training setup, Oh et al. [14] predict future frames in ATARI environments conditioned on actions. The predicted frames are used for learning the transition function of the environment, e.g. for improving exploration by informing agents of which actions are more likely to result in unseen states. Our work differs as we are acting within a learned latent space and not the full input space.

Visual planning

Variational State Tabulations [5] learn a state representation in addition to a transfer function over the latent space. However, their observation space is discretized into a table using a variational approach, as opposed to our continuous representation. Similarly, Cuccu et al. [54] discretize visual input using unsupervised vector quantization and use that representation for learning controllers for Atari games.

Inspired by classic symbolic planning, Regression Planning Networks [41] create a plan backwards from a symbolic goal. We do not have access to high-level symbolic goal information for our method and we assume that only high-dimensional visual cues are received from the environment.

Topological memories of the environment are built in Semi-parametric Topological Memories [55] after a manual exploration. Nodes are connected if a predictor estimates that they are close. The method has problems with generalization which are reduced in Hallucinative Topological Memories [56] where the method also admits a description of the environment, such as a map or a layout vector, which the agent can use during planning. Our visual planning method does not receive any additional information on unseen environments and does not depend on manual exploration during training.

Representation learning

Causal InfoGAN [20] is a method based on generative adversarial networks (GANs) [21], inspired by InfoGAN in particular [22], for learning a plannable representation. A GAN is trained for encoding start and goal states and they plan a trajectory in the representation space as well as reconstructing intermediate observations in the plan. Our method is different as it learns the representation as well as the forward model end-to-end, giving up the need for reconstruction. In Predictable Feature Analysis [17],

representations are learned that are predictable by autoregression processes. Our method is more flexible and scales better to higher dimensions as the predictor can be any differentiable function.

Using the output of other networks as prediction targets instead of the original pixels is not new. The case where the output of a larger model is the target for a smaller model is known as knowledge distillation [16] [18]. This is used for compressing a model ensemble into a single model. Vondrick et al. [19] learn to make high-level semantic predictions of future frames in video data. Given a frame at a current time, a neural network is tasked with predicting the representation of a future frame. Our approach is not constrained only to pre-trained representations, we learn our representation together with the prediction network. Moreover, we extend this general idea by also admitting an action as the input to our predictor network.

Materials and methods

In this work we study different representations for learning the transition function of a POMDP and propose a network that jointly learns a representation with a prediction model and apply it for latent space planning. We summarize here the different ingredients of LARP networks – our proposed solution.

Training the predictor network: We use a two-stream fully connected neural network (see S2 Appendix for details) to predict the representation of the future state given the current state’s representation and the action bridging those two states. The predictor module is trained with a simple mean-squared error term.

Handling constant solutions: The representation could be transferred from other domains or learned from scratch on the task. If the representation is learned simultaneously with an estimation of the POMDP’s transition function, precautions must be taken such that the prediction loss is not trivially minimized by a representation that is constant over all states. We consider three approaches for tackling the problem: spherizing the output, regularizing with a contrastive loss term, and regularizing with a reconstructive loss term.

Searching in the latent space: Combining the representation with the predictor network, we can search in the latent space until a node is found that has the largest similarity to the representation of the goal viewpoint using a modified best-first search algorithm.

NORB environment: We use the NORB data set for our experiments. This data set consists of images of objects from different viewpoints and we create viewpoint-matching tasks from the data set.

On good representations

We rely on heuristics to provide sufficient evidence for a good — albeit not necessarily optimal — decision at every time step to reach the goal. Here we use the Euclidean distance in representation space: a sequence of actions is preferred if their end location is closest to the goal. The usefulness of this heuristics depends on how well and how coherently the Euclidean distance encodes the actual distance to the goal state in terms of the number of actions.

A learned predictor network estimates the transition function of the environment for planning in the latent space defined by some representation. This raises the question: what is the ideal representation for latent space planning? Our experiments show that an openly available, general-purpose representation, such as a pre-trained VGG16 [26], can already provide sufficient guidance to apply such heuristics effectively.

One might, however, ask what a particularly suited representation might look like when attainability is ignored. It would need to take the topological structure of the underlying data manifold into account, such that the Euclidean distance becomes a good proxy for the geodesic distance. One class of methods that satisfy this are spectral embeddings, such as Laplacian Eigenmaps (LEMs) [27]. Their representations are smooth and discriminative which is ideal for our purpose. However, they do not easily produce out-of-sample embedding, so they will only be applied in an in-sample fashion to serve as a control experiment – and we actually get perfect performance with LEMs.

Predictor network

As the representation is used by the predictor network, we want them to be predictable. Thus, we optimize the representation learner simultaneously as we train the predictor network, in an end-to-end manner.

Suppose we have a representation map ϕ and a training set of N labeled data points $(X_i = [O_t, A_t], Y_i = O_{t+1})$, where O_t is the observation at time step t and A_t is an action resulting in a state with observation O_{t+1} . We train the predictor f , parameterized by θ , by minimizing the mean squared error loss over f 's parameters:

$$\operatorname{argmin}_{\theta} \mathcal{L}_{\text{prediction}}(D, \theta) = \operatorname{argmin}_{\theta} \frac{1}{N} \sum_{i=1}^N \|\phi(O_{t+1}) - f_{\theta}(\phi(O_t), A_t)\|^2 \quad (1)$$

where $D = \{(X_i, Y_i)\}_{i=0}^N$ is our set of training data.

We construct f as a two-stream, fully connected, neural network (S2 Appendix). Using this predictor we can carry out planning in the latent space defined by ϕ . By planning we mean that there is a start state with observation O_{start} and a goal state with O_{goal} and we want to find a sequence of actions connecting them.

The network outputs the expected representation after acting. Using this, we can formulate planning as a classical pathfinding or graph traversal problem.

Battling trivial solutions

In the case where ϕ is trainable and parameterized by η , the loss for the whole system that only cares about maximizing predictability is

$$\operatorname{argmin}_{\theta, \eta} \mathcal{L}_{\text{prediction}}(D, \theta, \eta) = \operatorname{argmin}_{\theta, \eta} \frac{1}{N} \sum_{i=1}^N (\phi_{\eta}(O_{t+1}) - f_{\theta}(\phi_{\eta}(O_t), A_t))^2 \quad (2)$$

for a given data set D . With no constraints on the family of functions that ϕ can belong to, we run the risk that the representation collapses to a constant. Constant functions $\phi = c$ trivially yield zero loss for any set D if f_{θ} outputs the input state again for any A , i.e $f(\phi(\cdot), A) = \phi(\cdot)$:

Constant representations are optimal with respect to predictability but they are unfortunately useless for planning, as we need to discriminate different states. This objective is not present in the proposed loss function in Eq. (2) and we must thus add a constraint or another loss term to facilitate disentangling the different states.

There are several ways to limit the function space such that constant functions are not included, for example with decoder [33] or adversarial [32] loss terms. In this work we do this with a spherling layer, a contrastive loss, or a reconstructive loss.

Spherling the output

The problem of trivial solutions is solved in Slow Feature Analysis [42] and related methods [2] [35] by constraining the overall covariance of the output to be I . Including

this constraint to our setting yields the optimization formulation:

$$\begin{aligned}
& \underset{\eta, \theta}{\text{minimize}} \quad \mathcal{L}_{\text{prediction}}(D, \theta, \eta) \\
& \text{subject to} \quad \mathbb{E}_D [\phi_\eta] = 0 \quad (\text{zero mean}) \\
& \quad \quad \quad \mathbb{E}_D [\phi_\eta \phi_\eta^T] = I \quad (\text{unit covariance})
\end{aligned} \tag{3}$$

We enforce this constraint in our network via architecture design. The last layer performs differentiable spherling [2] [50] of the second-to-last layer's output using the whitening matrix \mathbf{W} . We get \mathbf{W} using power iterations from the following iterative formula:

$$\mathbf{u}^{[i+1]} = \frac{\mathbf{T}\mathbf{u}^{[i]}}{\|\mathbf{T}\mathbf{u}^{[i]}\|} \tag{4}$$

Which converges to the largest eigenvector \mathbf{u} of a matrix \mathbf{T} in a few hundred, quick iterations. The eigenvalue λ is determined and we subtract the eigenvector from the matrix:

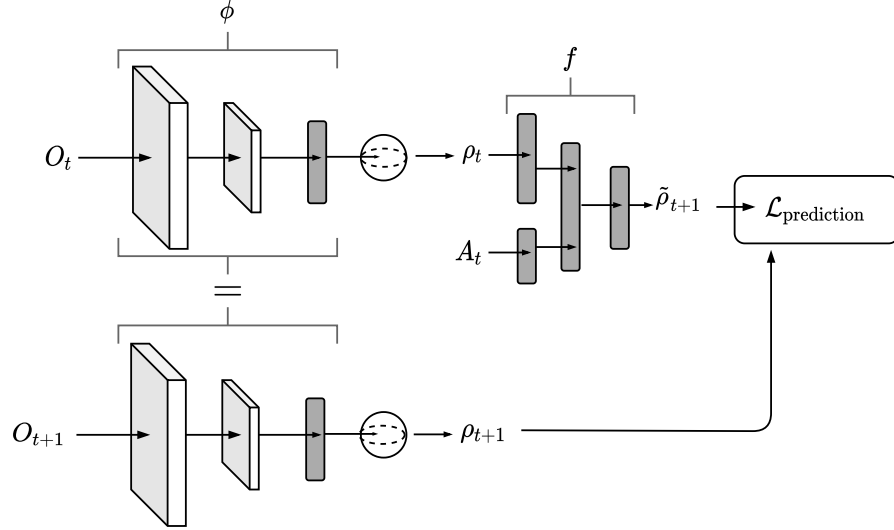
$$\mathbf{T} \leftarrow \mathbf{T} - \lambda \mathbf{u} \mathbf{u}^T \tag{5}$$

and the process is repeated until the spherling matrix is found

$$\mathbf{W} = \sum_{j=0}^1 \frac{1}{\sqrt{\lambda_j}} \mathbf{u}_j \mathbf{u}_j^T \tag{6}$$

The whole system, including the spherling layers, can be seen in Fig 2.

Fig 2. Predictive representation learning with spherling regularization. The observations O_t , and the resulting observation O_{t+1} after the action A_t is performed in O_t , are passed through the representation map ϕ , whose outputs are passed to a differentiable spherling layer before being passed to f . The predictive network f minimizes the loss function \mathcal{L} , which is the mean-squared error between $\phi(O_t) = \rho_t$ and $\phi(O_{t+1}) = \rho_{t+1}$.



Contrastive loss

Constant solutions can also be dealt with in the loss function instead of via architecture design. Hadsell et al. [3] propose to solve this with a loss function that pulls together

the representation of similar objects (in our case, states that are reachable from each other with a single action) but pushes apart the representation of dissimilar ones:

$$L_{\text{contrastive}}(O, O') = \begin{cases} \|\phi(O) - \phi(O')\| & \text{if } O, O' \text{ are similar} \\ \max(0, M - \|\phi(O) - \phi(O')\|) & \text{otherwise} \end{cases} \quad (7)$$

where M is a margin and $\|\cdot\|$ is some — usually the Euclidean — norm. The representation of dissimilar objects is pushed apart only if the inequality

$$\|\phi(O) - \phi(O')\| < M \quad (8)$$

is violated. During each training step, we compare each observation to a similar and a dissimilar observation simultaneously [30] by passing a triplet of (positive, anchor, negative) observations during training to three copies of ϕ . In our experiments, the positive corresponds to the predicted embedding of O_{t+1} given O_t and A_t , the anchor is the true resulting embedding after an action A_t is performed in state O_t and the negative is any other embedding that is not reachable from $\phi(O_t)$ with a single action. We define the next-step prediction $\tilde{\rho}_{t+1} := f(\phi(O_t), A_t)$ for readability and minimize:

$$\mathcal{L}_{\text{contrastive}}(O_t, O_{t+1}, O_n, A_t) = \|\phi(O_{t+1}) - \tilde{\rho}_{t+1}\| + \max(0, M - \|\phi(O_{t+1}) - \phi(O_n)\|) \quad (9)$$

It would seem that $\phi(O_{t+1})$ and $\tilde{\rho}_{t+1}$ are interchangeable since the second term is included only to prevent the representation from collapsing into a constant. However, if the loss function is

$$\mathcal{L}_{\text{contrastive}}(O_t, O_{t+1}, O_n, A_t) = \|\phi(O_{t+1}) - \tilde{\rho}_{t+1}\| + \max(0, M - \|\tilde{\rho}_{t+1} - \phi(O_n)\|) \quad (10)$$

then the network is rewarded during training for making f poor at predicting the next representation instead of simply pushing the representation of O_t and O_n away from each other.

There are two main ways to set the margin M , one is dynamically determining it per batch [29]. The other, which we choose, is constraining the representation to be on a hypersphere using L_2 normalization and setting a small constant margin such as $m = 0.2$ [30]. The architecture for the training scheme using the contrastive loss regularization is depicted in Fig. 3.

Reconstructive loss

Trivial solutions are avoided by Goroshin et al. [33] by introducing a decoder network D to a system that would otherwise converge to a constant representation. We incorporate this intuition into our framework with the loss function

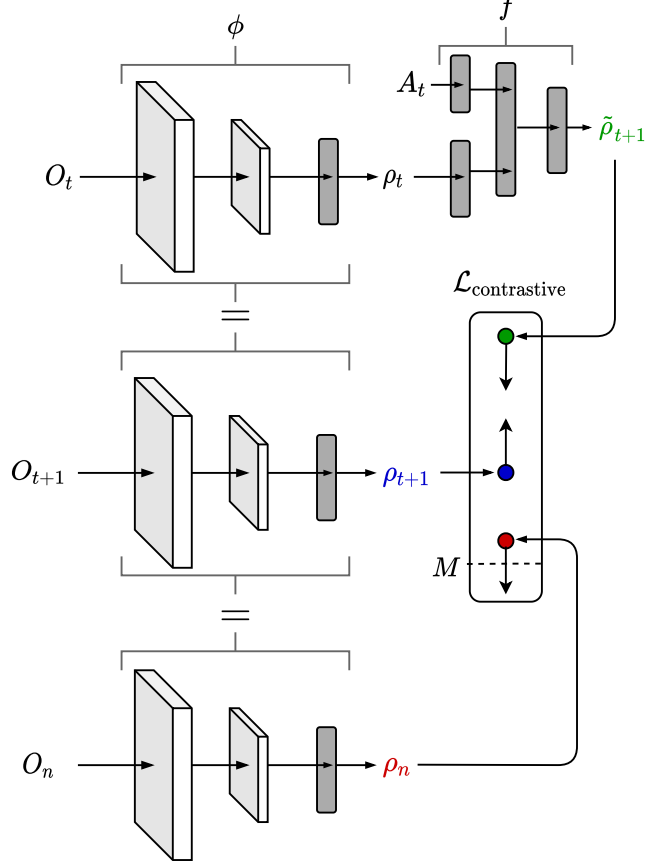
$$\begin{aligned} \mathcal{L}_{\text{decoder}}(O_t, O_{t+1}, A_t) &= \mathcal{L}_{\text{prediction}}(O_t, O_{t+1}) + \mathcal{L}_{\text{reconstruction}}(O_t, O_{t+1}) \\ &= (\phi(O_t) - \tilde{\rho}_{t+1})^2 + \alpha(O_{t+1} - D(\tilde{\rho}_{t+1}))^2 \end{aligned} \quad (11)$$

The desired effect of the regularization can also be achieved by replacing the second term in Eq. (11) with $\alpha(O_{t+1} - D(\phi(O_{t+1})))^2$. By doing this we would maximize the reconstructive property of the latent code in and of itself. We instead add an another level of predictive power in f : in addition to predicting the next representation, its prediction must also be useful in conjunction with the decoder D for reconstructing the new true observation.

This approach can add the largest computational overhead of the three, depending on the size of the decoder. We construct the decoder network D such that it closely mirrors the architecture of ϕ , with convolutions replaced by transposed convolutions and max pooling replaced by upsampling.

Fig 3. Predictive representation learning with contrastive loss

regularization. We minimize the contrastive loss function (Eq. 9), depicted in the rightmost box. The predicted future representation $\tilde{\rho}_{t+1}$ is pulled towards the next step’s representation ρ_{t+1} . However, ρ_{t+1} is pushed away from the negative state’s representation ρ_n if the distance between them is less than M . The observation O_n is randomly selected from those that are not reachable from O_t with a single action.



Training and architecture of the predictor network

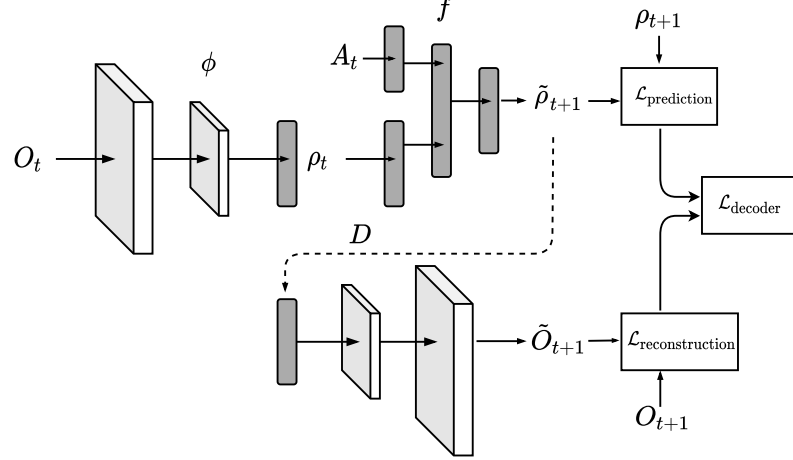
We train the representation network and predictor network jointly by minimizing Eq. (2), Eq. (10) or Eq. (12). The details of the network architectures can be found in S2 Appendix. The predictor network can also be trained on its own for a fixed representation map ϕ . In this case, f is tasked as before with predicting $\phi(O_{t+1})$ after the action A is performed in the state with observation O_t by minimizing the mean-squared error between $f(\phi(O_t), A_t)$ and $\phi(O_{t+1})$. The networks are built with Keras [37] and optimized with rmsprop [53].

Planning in transition-learned domain representation space

We use a modified best-first search algorithm with the trained representations for our experiments (Algorithm 1). From a given state, the agent performs a mental exploration for the goal state. At the start state, the agent estimates the resulting representation after each action. Out of those representations, starting with the one closest to the goal representation, the agent repeats the process until a maximum number of trials is made.

Each observation is associated with a node as well as a score: the distance between

Fig 4. Predictive representation learning with decoder loss regularization. The $\mathcal{L}_{\text{prediction}}$ and $\mathcal{L}_{\text{decoder}}$ boxes both return the mean-squared error of their inputs and the full loss $\mathcal{L}_{\text{total}}$ is the sum of those two terms.



its representation and the representation of the goal observation. The edges between nodes are the available actions at each state. The output of the search is the sequence of actions that corresponds to the path connecting the start node to the proposed solution node, i.e. the node whose representation is the one closest to the goal.

Algorithm 1 From a given starting state S_{start} , find a plan to reach the state corresponding to $O_{\text{result}} = O_j$, where $j = \operatorname{argmin}_{i \leq k} \|\rho_i - \phi(O_{\text{goal}})\|$ and $\rho = \{\rho_1, \dots, \rho_k\}$ is a set of the representations of searched states.

Require: O_{start} , O_{goal} , trials m , action set \mathcal{A} , representation map ϕ and predictor f
Ensure: A plan of actions (A_0, \dots, A_n) reaching $O_{\text{result}} \approx O_{\text{goal}}$ from O_{start}

```

 $\rho \leftarrow \emptyset, A \leftarrow \emptyset, D \leftarrow \emptyset, p_0 \leftarrow \emptyset, P \leftarrow \emptyset$ 
 $\rho_0 \leftarrow \phi(O_{\text{start}})$ 
for  $k \leftarrow 0$  to  $m$  do
   $j = \operatorname{argmin}_{i \leq k, i \notin D} \|\rho_i - \phi(O_{\text{goal}})\|$  # take a new state, most similar to the goal
  for all  $A \in \mathcal{A}$  do
     $\rho_{k+1} \leftarrow f(\rho_j, A)$  # try every action from current state
     $\rho \leftarrow \rho \cup \{\rho_{k+1}\}$  # save the estimated representation
     $P_{k+1} \leftarrow P_j \cup A$ 
     $P \leftarrow P \cup \{P_{k+1}\}$  # store path from goal state to current state
     $k \leftarrow k + 1$ 
  end for
   $D \leftarrow D \cup j$  # add j to the set of checked indices
end for
return  $P_j$ 

```

To make the algorithm faster, we only consider paths that do not take us to a state that has already been evaluated, even if there might be a difference in the predictions from going this roundabout way. That is, if a permutation of the actions in the next path to be considered is already in an evaluated path, it will be skipped. This has the same effect as transposition tables used to speed up search in game trees. Paths might be produced with redundancies, which can be amended with path-simplifying routines (e.g. take one step forward instead of one step left, one forward then one right).

We do Model-Predictive Control [36], that is, after a path is found, one action is

performed and a new path is recalculated, starting from the new position. Since the planning is possibly over a long time horizon, we might have a case where a previous state is revisited. To avoid loops resulting from this, we keep track of visited state-action pairs and avoid an already chosen action for a given state.

NORB viewpoint-matching experiments

For our experiments, we create an OpenAI Gym environment based on the small NORB data set [1]. The code for the environment is available at <https://github.com/wiskott-lab/gym-norb> and requires the pickled NORB data set hosted at <https://s3.amazonaws.com/unsupervised-exercises/norb.p>. The data set contains 50 toys, each belonging to one of five categories: four-legged animals, human figures, airplanes, trucks, and cars. Each object has stereoscopic images under six lighting conditions, 9 elevations, and 18 azimuths (in-scene rotation). In all of the experiments, we train the methods on nine car class toys, testing on the other toys.

Each trial in the corresponding RL environment revolves around a single object under a given lighting condition. The agent is presented with a start and a goal viewpoint of the object and transitions between images until the current viewpoint matches the goal where each action operates the camera. To be exact, the actions correspond to turning a turntable back and forth by 20° , moving the camera up or down by 5° and, in one experiment, changing the lighting. The trial is a success if the agent manages to change viewpoints from the start position until the goal viewpoint is matched in fewer than twice the minimum number of actions necessary.

We compare the representations learned from the three different loss functions as well as two fixed ones, namely the Laplacian Eigenmaps and the second-to-last layer of the VGG16 pre-trained on ImageNet [39]. As fixed representations do not change throughout the training, they can be saved to disk, speeding up the training. As a reference, we consider three reinforcement learning methods: (1) a Deep Q-Networks (DQN) [51], (2) Proximal Policy Optimization (PPO) [52] and (3) World Models [15].

The data set is turned to a graph for search by setting each image as a node and each viewpoint-changing action as an edge. The task of the agent is to transition between neighboring viewing angles until a goal viewpoint is reached. The total number of training samples is fixed to 25600. For our method, a sample is a single (O_t, O_{t+1}, A_t) triplet to be predicted while for the regular RL methods it is a $(O_t, O_{t+1}, A_t, \rho_t)$.

Results

With our empirical evaluation we aim to answer the following questions:

- Is training a representation for predictability feasible?
- In terms of planning performance, what are the best restrictions to place on the representation to avoid trivial solutions?
- Is the Euclidean distance of a representation and the goal representation similar to the number of actions that separate them?
- How does planning with LARP compare to other methods from the RL literature?
- What is the best size of the latent space for our planning tasks?
- How does our method generalize to different environments?
- How is the performance of our method affected when we place obstacles in trained environments?

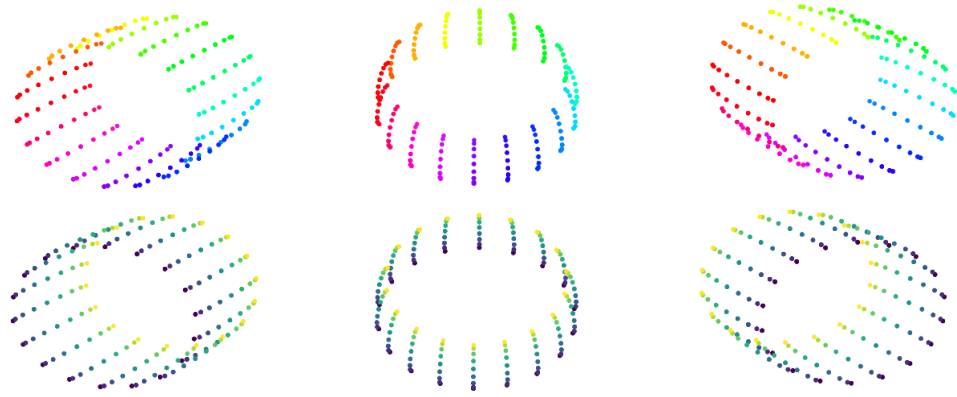


Fig 5. Laplacian Eigenmap representation space of a NORB toy. The three-dimensional Laplacian Eigenmaps of a toy car with azimuth (top) or elevation (bottom) colored in. Euclidean distance is a good substitute for geodesic distance in this case.

Latent space visualization

When the representation and predictor networks are trained, we apply Algorithm 1 to the viewpoint-matching task. As described above, the goal is to find a sequence of actions that connects the start state to the goal state, where the two states differ in their configurations.

To support the qualitative analysis of the latent space, we plot similarity heatmaps of nodes during search (Fig 7). Of the 10 car toys in the NORB data set, we randomly chose 9 for our training set and test on the remaining one.

In-sample embedding: Laplacian Eigenmaps

In order to get the best-case representation, we embed the toy using Laplacian Eigenmaps. Embedding a single toy in three dimensions using Laplacian Eigenmaps results in a tube-like embedding that encodes both elevation and azimuth angles, see Fig 5. Three dimensions are needed, so that the cyclic azimuth can be embedded correctly as $\sin(\theta)$ and $\cos(\theta)$.

If the representation is now used to train the predictor, one would expect that the representation becomes monotonically more similar to the goal representation as the state moves towards the goal. In Fig 6 we see that this is the case and that this behavior can be effectively used for a greedy heuristics. While the monotonicity is not always exact due to errors in the prediction, Fig 6 still qualitatively illustrates a best-case scenario.

Out-of-sample embedding: pre-trained VGG16 representation

Next we consider the pre-trained representation of the VGG16 network to get a representation that generalizes to new objects. We plot the heat map of the predicted similarity between each state and the goal state, beginning from the start state, in Fig 7.

The heat maps of the type shown in Fig. 7 can be grouped to show basins of attraction during the search. Each heat map is shifted such that the goal position is at the bottom, middle row (Fig 8, a). Here it is obvious that the goal and the 180° flipped (azimuth) version of the goal are attractor states. This is due to the representation map being sensitive to the rough shape of the object, but being unable to distinguish finer

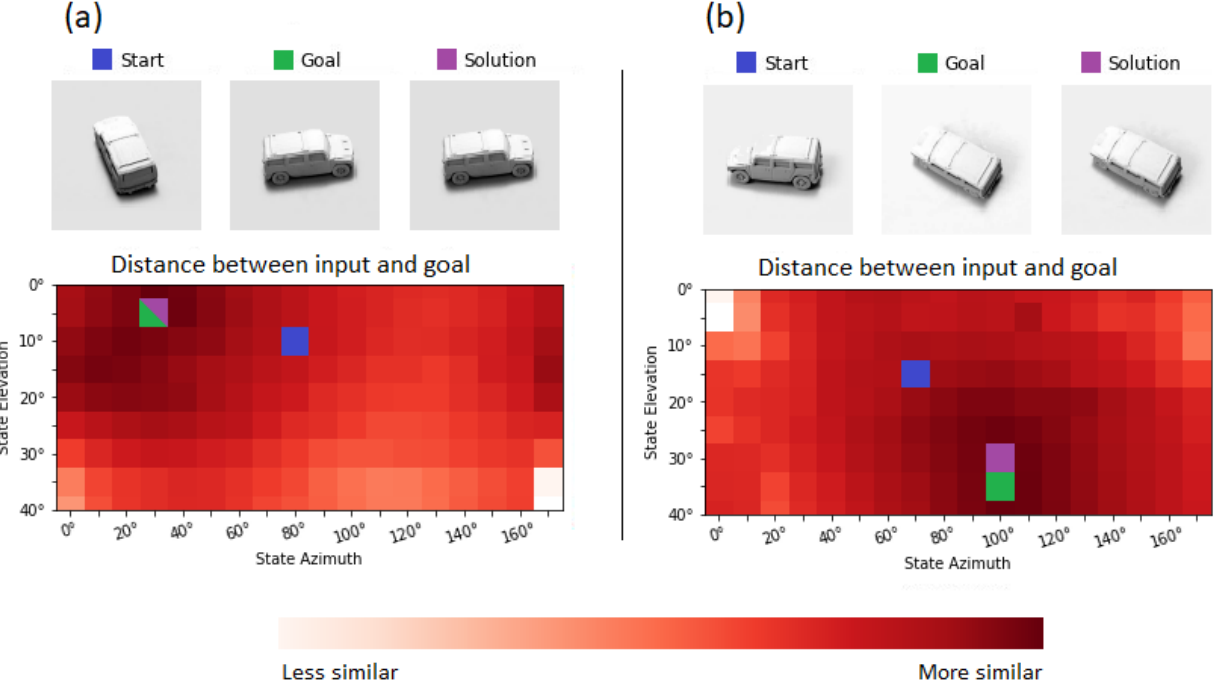


Fig 6. Heatmap of Laplacian Eigenmap latent space similarity. Only the start and goal observations are given. The blue dot shows the start state, green the goal, and purple the solution state found by the algorithm. The search algorithm can depend on an almost monotonously decreasing distance between the each state’s predicted representation and the goal’s representation to guide its search.

details. In (Fig 8, b) we display an aggregate heat map when the agent can also change the lighting conditions.

Our visualizations show a gradient towards the goal state in addition to a visually similar far-away-states. Prediction errors prevent the planning algorithm from finding the exact goal for every task, sometimes producing solutions that are the polar-opposite of the goal with respect to the azimuth.

To investigate the accuracy of the search with respect to each dimension separately, we plot the histogram in Fig 9. The goal and start states are chosen randomly, with the restriction that the azimuth distance and elevation distance between them are each uniformly sampled. For the rest of the paper, all trials follow this sampling procedure. The results look less accurate for elevation than azimuth, because the elevation changes are smaller than the azimuth changes. The difference between the goal and solution viewpoints in Fig 7 left, for example, is hardly visible. If one would scale the histograms by angle and not by bins, the drop-off would be similar.

Latent space dimensionality

We do an ablation study of the dimensionality of the representation for our method (Table 1). The test car is an unseen car toy from the NORB data set and the train car comes from the training set.

There is no complete and total winner: the network with the spherling layer does the best on one of the cars used during training while the reconstructive-loss network does the best on the held-out test car. The sharp difference in performance between 64 and 94 spherling-regularized representation can be explained by the numerical instability of

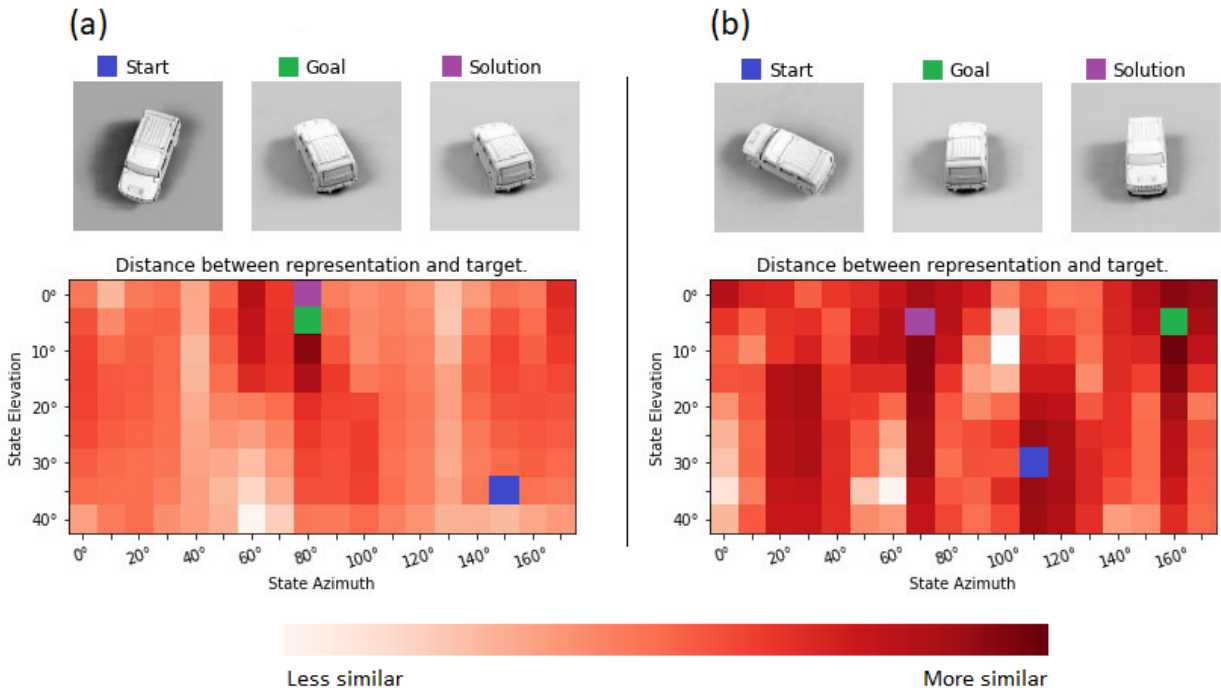


Fig 7. Heatmap of VGG16 latent space similarity. The predictor network estimates the VGG16 representation of the resulting states as the object is manipulated. **(a)** The goal lies on a hill containing a maximum of representational similarity. **(b)** The accumulated errors of iterated estimations cause the algorithm to plan a path to a wrong state with a similar shape.

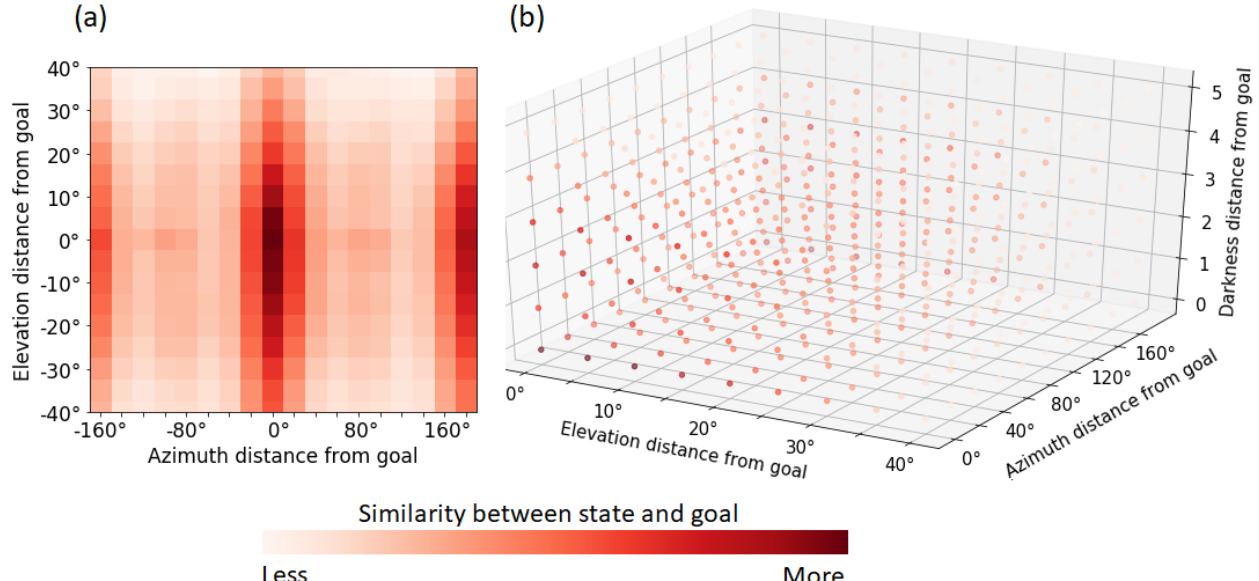


Fig 8. Aggregate heat maps of representation similarities on test data. The data is collected as the state space is searched for a matching viewpoint. The pixels are arranged according to their elevation and azimuth difference from the goal state at $(0^\circ, 0^\circ)$ on the left and $(0^\circ, 0^\circ, 0^\circ)$ on the right. (a) We see clear gradients towards the two basins of attraction. There is less change along the elevation due to less change at each step. (b) The agent can also change the lighting of the scene, with qualitatively similar results. In this graphic we only measure the absolute value of the distance.

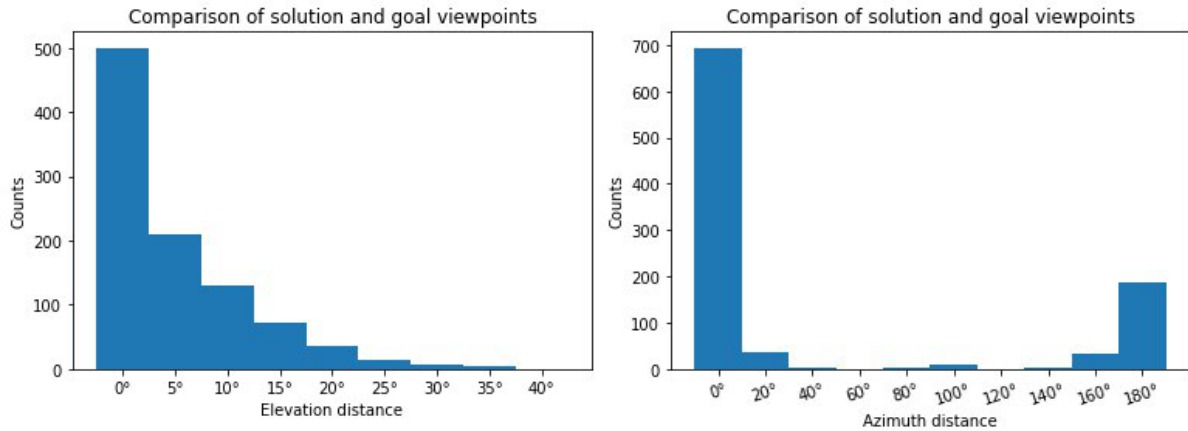


Fig 9. Histograms of elevation-wise and azimuth-wise errors. The histograms display the counts of the distance between goal and solution states along elevation (left) and azimuth (right) on test data. The distance between the start and goal viewpoints is equally distributed across all the trials, along both dimensions. The goal and the 180° flipped (azimuth) version of the goal are attractor states.

Table 1. Ablation study of the representation dimensionality. We change the output dimension of the representation learner subnetwork and compare it to the VGG16 representation trained on ImageNet. The performance is averaged over a hundred trials of the viewpoint-matching task.

Representation	Dimension	Test Car (%)	Train Car (%)
Contrastive	96	56.8 \pm 0.3	59.3 \pm 0.3
	64	60.5 \pm 0.3	64.1 \pm 0.3
	32	59.4 \pm 0.3	72.3 \pm 0.3
	16	59.3 \pm 0.3	74.1 \pm 0.2
	8	58.0 \pm 0.3	82.7 \pm 0.2
Sphering	96	37.8 \pm 0.3	41.1 \pm 0.3
	64	53.7 \pm 0.3	93.9\pm0.1
	32	51.9 \pm 0.3	89.8 \pm 0.1
	16	42.6 \pm 0.3	85.2 \pm 0.2
	8	40.1 \pm 0.3	85.1 \pm 0.1
Decoder	96	51.9 \pm 0.3	58.0 \pm 0.3
	64	63.0\pm0.3	79.5 \pm 0.3
	32	61.7 \pm 0.3	77.8 \pm 0.3
	16	45.2 \pm 0.3	51.9 \pm 0.3
	8	42.4 \pm 0.3	51.1 \pm 0.3
VGG16	902	55.1 \pm 0.3	62.4 \pm 0.2
Random Steps		3.5 \pm 0.0	3.5 \pm 0.0

the power iteration method for too large matrix dimensions.

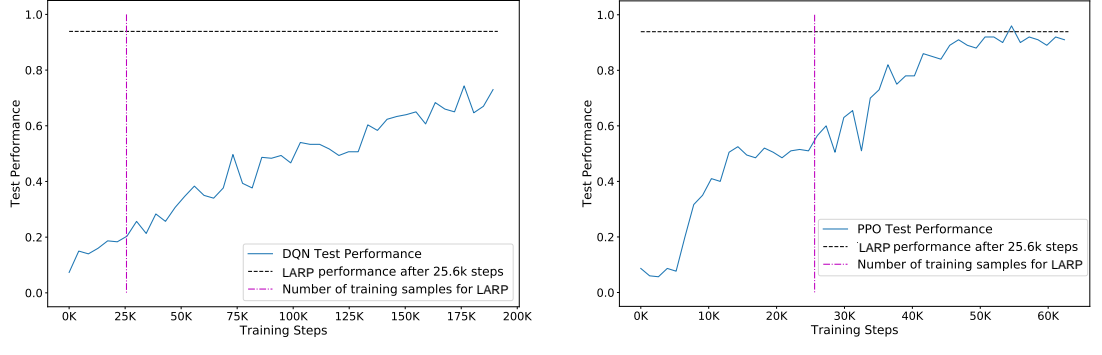
The VGG16 representation is not the highest performer on any of the car toys. Many of the representation values are 0 for all images in the NORB data set, so we only use those that are nonzero for any of the images. We suggest that this high number of dead units is due to the representation being too general for the task of manipulating relatively homogenous objects. A drawback of using pre-trained networks is that information might be encoded that is unimportant for the task. This has the effect that our search method is not guaranteed to output the correct solution in the latent space, as there might be distracting pockets of local minima.

The random baseline has an average success rate of 3.5%, which is very clearly outperformed by our method. As 64 is the best dimensionality for the representation on average, we continue with that number for our method in the transfer learning experiment.

Comparison with other RL methods

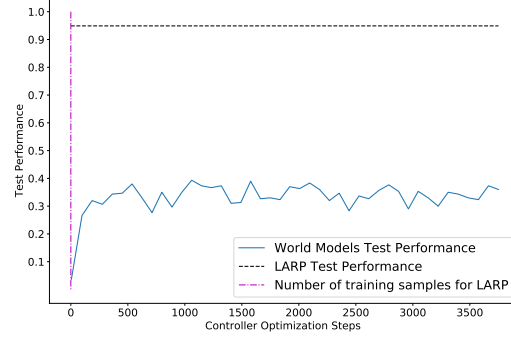
For the comparison with standard RL methods, we use the default configurations of the model-free methods DQN and PPO as defined in OpenAI Baselines [45] and compare them with our method on the car viewpoint-matching task (Fig. 10). We make sure that the compared RL methods are similar to our system in terms of the number of parameters as well as architecture layout. Our model-based comparison is chosen to be world models [15] from <https://github.com/zacwellmer/WorldModels>.

The DQN networks are much more sample inefficient than PPO, which in turn is more sample inefficient than our method. However, our method is more time-consuming during test time. We require a forward pass of the predictor network for each node that is searched before we take the next step, contrasted with a single pass in total of the



(a) DQN Performance.

(b) PPO Performance.



(c) World Models Performance.

Fig 10. Reinforcement learning comparison. Each data point is the mean of 100 test episodes, averaged over 5 different seeds of both learners. In (a) and (b), the vertical line indices the number of training samples for ours and the horizontal line shows our performance at that point. The models in (c) are trained on 25.6k transitions, as described in the paper by Ha et al., and the plot shows the optimization curve for the controller.

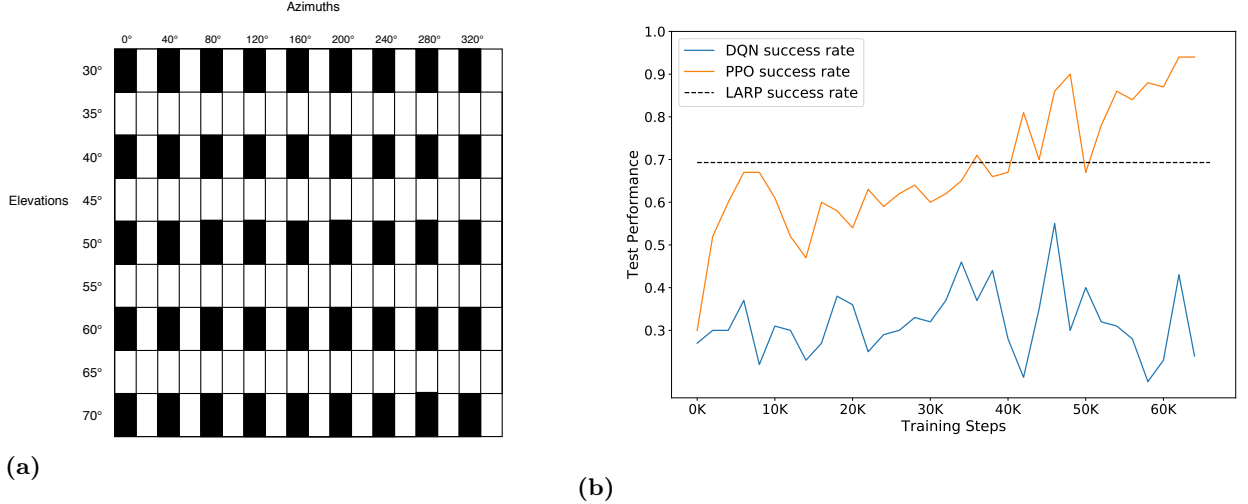


Fig 11. Re-training after placing checkerboard-patterned obstacles. (a) The task is the same as before, but nothing happens if the agent attempts to move to a state containing a black rectangle. (b) After training the agents, we re-tested them after we introduced the checkerboard pattern of obstacles. Our method does not allow for re-training in the new environment.

DQN / PPO networks for the next step.

Our method reaches 93.9% success rate on the train car (Table 1) using 25.6k samples, but the best PPO run only reaches 70.5% after training on the same number of samples. The best single PPO run needed 41.3k samples to get higher than 93.9% success rate and the average performance is higher than 93.9% at around 55k samples. After that, some PPO learners declined again in performance.

World models quickly reaches the same level of performance as DQN got after 50k steps and PPO after approximately 8k steps, but it doesn't improve beyond that.

Modifying the environment

To see how the methods compare when obstacles are introduced to the environment, we repeat the trial on one of the car objects except that the agent can no longer pass through states whose elevation values are divisible by 10 and azimuth values are divisible by 40 (Fig. 11, (a)).

As before, the goal and start locations can have any azimuth-elevation pair but the agent cannot move into states with the properties indicated by the black rectangle. Every action is available to the agent at all locations as before, but the agent's state is unchanged if it attempts to move to a state with a black rectangle.

We trained LARP using the contrastive loss, PPO and DQN agents until they reached 80% accuracy on our planning task and then tested them with the added obstacles. Our method loses about 10% performance, but PPO loses 50%. Nevertheless, we can continue training PPO until it quickly reaches top performance again (Fig. 11, (b)). Our method is not re-trainable for the new task and DQN did not reach a good performance again in the time we allotted for re-training.

Transfer to dissimilar objects

Selecting the best dimensionality for the representation from the previous set of experiments, we investigate further their performance in harder situations using unseen,

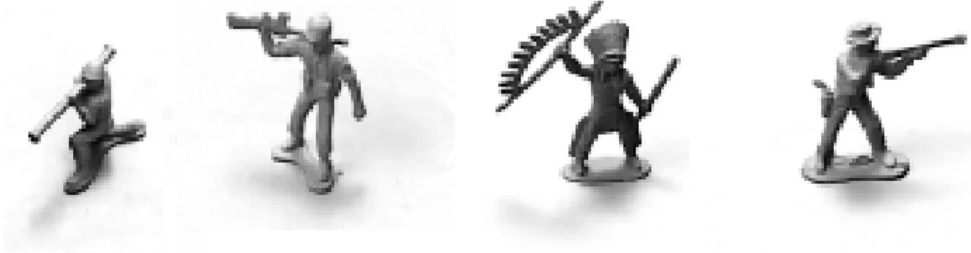


Fig 12. Toys for transfer learning experiments. From left to right: Soldier (Kneeling), Soldier (Standing), Native American with Bow and Cowboy with Rifle.

Table 2. Transfer learning performance. The methods are trained on the car object data and then their performance on dissimilar toys is tested. Each number is the mean success rate of viewpoint matching, with a standard deviation of 0.1, out of 100 trials.

Representation	Soldier (Kneeling)	Soldier (Standing)	Native American with Bow	Cowboy with Rifle
Contrastive	23	11	12.1	20.7
Sphering	18.4	15.3	15.2	15.8
Decoder	14.3	16.6	14.7	15.6
VGG16	12.3	12.9	11.8	13.6

non-car objects (Table 2)

Our experiments include the pre-trained VGG16 network because we believe that a flexible algorithm should rather be based on a generic multi-purpose-representation and not on a specific representation. To our surprise, it is outperformed by our approach on every object, even as the viewpoint-matching task is done on objects that are different from the original car toys they are trained on.

Discussion

In this work we present Latent Representation Prediction (LARP) networks with applications to visual planning. We jointly learn a model to predict transitions in a partially-observable Markov decision processes with a representation trained to be maximally predictable, allowing us to accurately search the latent space defined by the representation. We validate our method on a viewpoint-matching task derived from the NORB data set. Unsurprisingly, a representation that is optimized simultaneously with the predictor network performs the best in our experiments. A common issue of unsupervised representation learning is the one of trivial solutions: a constant representation which optimally solves the unsupervised optimization problem but brings across no information. To avoid the trivial solution we constrain the training by introducing a sphering layer or a loss term that is either contrastive or reconstructive.

Any of these approaches will do the job of preventing the representations from collapsing to constants, and none of them is displays absolute superiority over the others. Our LARP representation is competitive with pre-trained representations for planning and compares favorably to other reinforcement learning (RL) methods. Our approach is a sound solution for learning a meaningful representation that is suitable for planning only from interactions. The planning performance remains good even when

obstacles are introduced to the environment or when the representation is transferred to an unseen environment.

Furthermore, we find that our method is more sample-efficient during training than standard reinforcement learning methods and our learned representation and predictive model transfer to harder scenarios. However, a disadvantage of our method compared to standard RL methods is that the execution time of our method is longer, as a forward pass is calculated for each node during the latent space search.

Another advantage of our approach is that it is adaptable to any changes in the tasks. For example, our search would not be hindered if some obstacles were placed in the environment or some states were forbidden to traverse through. Furthermore, the reward or discount rates can be easily changed for our method while standard RL methods are usually restricted in their optimization problems. Often, there is a choice between optimizing discounted or undiscounted expected returns.

Simulation/rollout-based planning methods are not restricted in that sense: If reward trajectories can be predicted, one can optimize arbitrary functions of these and regularize behavior. For example, a risk-averse portfolio manager can prioritize smooth reward trajectories over volatile ones.

Future lines of work should investigate further the effect of the different constraints on the end-to-end learning of representations suited for a predictive forward model, as well as considering novel ones. The search algorithm can be improved and made faster, especially for higher-dimensional action spaces or continuous ones.

Supporting information

S1 Supplement Environment Code (ZIP)

S2 Appendix LARP Architectures and Code (PDF)

S3 Figure Train Cars Sample (PNG)

S4 Figure Test Car Sample (PNG)

Acknowledgments

We would like to thank Zahra Fayyaz, Simon Hakenes and Daniel Vonk for contributing to discussions related to this project.

Author contributions

Conceptualization: Hlynur Davíð Hlynsson, Tobias Glasmachers, Laurenz Wiskott

Data Curation: Hlynur Davíð Hlynsson, Merlin Schüler, Robin Schiewer

Formal Analysis: Hlynur Davíð Hlynsson, Merlin Schüler

Funding Acquisition: Laurenz Wiskott

Investigation: Hlynur Davíð Hlynsson

Methodology: Hlynur Davíð Hlynsson, Laurenz Wiskott

Project Administration: Hlynur Davíð Hlynsson

Resources: Laurenz Wiskott, Merlin Schüler

Software: Hlynur Davíð Hlynsson, Merlin Schüler, Robin Schiewer

Supervision: Laurenz Wiskott

Validation: Hlynur Davíð Hlynsson

Visualization: Hlynur Davíð Hlynsson, Robin Schiewer

Writing – Original Draft Preparation: Hlynur Davíð Hlynsson

Writing – Review & Editing: Hlynur Davíð Hlynsson, Laurenz Wiskott, Tobias Glasmachers, Merlin Schüler, Robin Schiewer

References

1. LeCun Y, Huang FJ, Bottou L, et al. Learning methods for generic object recognition with invariance to pose and lighting. In: CVPR (2). Citeseer; 2004. p. 97–104.
2. Schüler M, Hlynsson HD, Wiskott L. Gradient-based training of slow feature analysis by differentiable approximate whitening. arXiv preprint arXiv:180808833. 2018;.
3. Hadsell R, Chopra S, LeCun Y. Dimensionality reduction by learning an invariant mapping. In: 2006 IEEE Computer Society Conference on Computer Vision and Pattern Recognition (CVPR'06). vol. 2. IEEE; 2006. p. 1735–1742.
4. Wang X, Ma T, Ainooson J, Cha S, Wang X, Molla A, et al. The Toybox Dataset of Egocentric Visual Object Transformations. arXiv preprint arXiv:180606034. 2018;.
5. Corneil D, Gerstner W, Brea J. Efficient model-based deep reinforcement learning with variational state tabulation. arXiv preprint arXiv:180204325. 2018;.
6. Hamrick JB. Analogues of mental simulation and imagination in deep learning. Current Opinion in Behavioral Sciences. 2019;29:8–16.
7. Tamar A, Wu Y, Thomas G, Levine S, Abbeel P. Value iteration networks. In: Advances in Neural Information Processing Systems; 2016. p. 2154–2162.
8. Srinivas A, Jabri A, Abbeel P, Levine S, Finn C. Universal planning networks. arXiv preprint arXiv:180400645. 2018;.
9. Hafner D, Lillicrap T, Fischer I, Villegas R, Ha D, Lee H, et al. Learning latent dynamics for planning from pixels. arXiv preprint arXiv:181104551. 2018;.
10. Henaff M, Whitney WF, LeCun Y. Model-based planning with discrete and continuous actions. arXiv preprint arXiv:170507177. 2017;.

11. Chua K, Calandra R, McAllister R, Levine S. Deep reinforcement learning in a handful of trials using probabilistic dynamics models. In: Advances in Neural Information Processing Systems; 2018. p. 4754–4765.
12. Gal Y, McAllister R, Rasmussen CE. Improving PILCO with Bayesian neural network dynamics models. In: Data-Efficient Machine Learning workshop, ICML. vol. 4; 2016.
13. Gelada C, Kumar S, Buckman J, Nachum O, Bellemare MG. DeepMDP: Learning Continuous Latent Space Models for Representation Learning. arXiv preprint arXiv:190602736. 2019;.
14. Oh J, Guo X, Lee H, Lewis RL, Singh S. Action-conditional video prediction using deep networks in atari games. In: Advances in neural information processing systems; 2015. p. 2863–2871.
15. Ha D, Schmidhuber J. World models. arXiv preprint arXiv:180310122. 2018;.
16. Hinton G, Vinyals O, Dean J. Distilling the knowledge in a neural network. arXiv preprint arXiv:150302531. 2015;.
17. Richthofer S, Wiskott L. Predictable feature analysis In: 2015 IEEE 14th International Conference on Machine Learning and Applications (ICMLA). IEEE; 2015. p. 190–196.
18. Buciluă C, Caruana R, Niculescu-Mizil A. Model compression. In: Proceedings of the 12th ACM SIGKDD international conference on Knowledge discovery and data mining. ACM; 2006. p. 535–541.
19. Vondrick C, Pirsiavash H, Torralba A. Anticipating visual representations from unlabeled video. In: Proceedings of the IEEE Conference on Computer Vision and Pattern Recognition; 2016. p. 98–106.
20. Kurutach T, Tamar A, Yang G, Russell SJ, Abbeel P. Learning Plannable Representations With Causal InfoGAN. In: Advances in Neural Information Processing Systems; 2018. p. 8733–8744.
21. Goodfellow I, Pouget-Abadie J, Mirza M, Xu B, Warde-Farley D, Ozair S, et al. Generative adversarial nets. In: Advances in neural information processing systems; 2014. p. 2672–2680.
22. Chen X, Duan Y, Houthooft R, Schulman J, Sutskever I, Abbeel P. InfoGAN: Interpretable representation learning by information maximizing generative adversarial nets. In: Advances in neural information processing systems; 2016. p. 2172–2180.
23. Jeannerod M, Arbib M. Action monitoring and forward control of movements. The Handbook of Brain Theory and Neural Networks, 2003; p. 83–85.
24. Sharif Razavian A, Azizpour H, Sullivan J, Carlsson S. CNN features off-the-shelf: an astounding baseline for recognition. In: Proceedings of the IEEE conference on computer vision and pattern recognition workshops; 2014. p. 806–813.
25. Nilsson NJ. Principles of artificial intelligence. Morgan Kaufmann; 2014.
26. Simonyan K, Zisserman A. Very deep convolutional networks for large-scale image recognition. arXiv preprint arXiv:14091556. 2014;.

27. Belkin M, Niyogi P. Laplacian eigenmaps for dimensionality reduction and data representation. *Neural computation*. 2003;15(6):1373–1396.
28. Russell SJ, Norvig P. Artificial intelligence: a modern approach. Malaysia; Pearson Education Limited,; 2016.
29. Sun Y, Chen Y, Wang X, Tang X. Deep learning face representation by joint identification-verification. In: Advances in neural information processing systems; 2014. p. 1988–1996.
30. Schroff F, Kalenichenko D, Philbin J. Facenet: A unified embedding for face recognition and clustering. In: Proceedings of the IEEE conference on computer vision and pattern recognition; 2015. p. 815–823.
31. Harwood B, Kumar B, Carneiro G, Reid I, Drummond T, et al. Smart mining for deep metric learning. In: Proceedings of the IEEE International Conference on Computer Vision; 2017. p. 2821–2829.
32. Denton EL, et al. Unsupervised learning of disentangled representations from video. In: Advances in neural information processing systems; 2017. p. 4414–4423.
33. Goroshin R, Mathieu MF, LeCun Y. Learning to linearize under uncertainty. In: Advances in Neural Information Processing Systems; 2015. p. 1234–1242.
34. Xu D, Martín-Martín R, Huang DA, Zhu Y, Savarese S, Fei-Fei LF. Regression Planning Networks. In: Wallach H, Larochelle H, Beygelzimer A, d'Alché-Buc F, Fox E, Garnett R, editors. Advances in Neural Information Processing Systems 32. Curran Associates, Inc.; 2019. p. 1319–1329. Available from: <http://papers.nips.cc/paper/8413-regression-planning-networks.pdf>.
35. Escalante-B AN, Wiskott L. How to solve classification and regression problems on high-dimensional data with a supervised extension of slow feature analysis. *The Journal of Machine Learning Research*. 2013;14(1):3683–3719.
36. Garcia CE, Prett DM, Morari M. Model predictive control: theory and practice—a survey. *Automatica*. 1989;25(3):335–348.
37. Chollet F, et al.. Keras; 2015. <https://keras.io>.
38. Dozat T. Incorporating Nesterov momentum into ADAM. 2016;.
39. Deng J, Dong W, Socher R, Li LJ, Li K, Fei-Fei L. ImageNet: A large-scale hierarchical image database. In: 2009 IEEE conference on computer vision and pattern recognition. Ieee; 2009. p. 248–255.
40. Barreto A, Dabney W, Munos R, Hunt JJ, Schaul T, van Hasselt HP, et al. Successor features for transfer in reinforcement learning. In: Advances in neural information processing systems; 2017. p. 4055–4065.
41. Xu D, Martín-Martín R, Huang DA, Zhu Y, Savarese S, Fei-Fei LF. Regression Planning Networks. In: Wallach H, Larochelle H, Beygelzimer A, d'Alché-Buc F, Fox E, Garnett R, editors. Advances in Neural Information Processing Systems 32. Curran Associates, Inc.; 2019. p. 1319–1329. Available from: <http://papers.nips.cc/paper/8413-regression-planning-networks.pdf>.
42. Wiskott L, Sejnowski TJ. Slow feature analysis: Unsupervised learning of invariances. *Neural computation*. 2002;14(4):715–770.

43. Sprikeler H. On the relation of slow feature analysis and laplacian eigenmaps. *Neural computation*. 2011;23(12):3287–3302.
44. Du SS, Kakade SM, Wang R, Yang LF. Is a Good Representation Sufficient for Sample Efficient Reinforcement Learning? arXiv preprint arXiv:191003016. 2019;;
45. Dhariwal P, Hesse C, Klimov O, Nichol A, Plappert M, Radford A, et al.. OpenAI Baselines; 2017. <https://github.com/openai/baselines>.
46. Saphal R, Ravindran B, Mudigere D, Avancha S, Kaul B. SEERL: Sample Efficient Ensemble Reinforcement Learning. arXiv preprint arXiv:200105209. 2020;;
47. Wang Z, Bapst V, Heess N, Mnih V, Munos R, Kavukcuoglu K, et al. Sample efficient actor-critic with experience replay. arXiv preprint arXiv:161101224. 2016;;
48. Hlynsson HD, ANE, Wiskott L. Measuring the Data Efficiency of Deep Learning Methods. In: Proceedings of the 8th International Conference on Pattern Recognition Applications and Methods - Volume 1: ICPRAM,. INSTICC. SciTePress; 2019. p. 691–698.
49. Buckman J, Hafner D, Tucker G, Brevdo E, Lee H. Sample-Efficient Reinforcement Learning with Stochastic Ensemble Value Expansion. In: Bengio S, Wallach H, Larochelle H, Grauman K, Cesa-Bianchi N, Garnett R, editors. Advances in Neural Information Processing Systems 31. Curran Associates, Inc.; 2018. p. 8224–8234. Available from: <http://papers.nips.cc/paper/8044-sample-efficient-reinforcement-learning-with-stochastic-ensemble-value-expansion.pdf>.
50. Hlynsson HD, Wiskott L. Learning Gradient-Based ICA by Neurally Estimating Mutual Information. In: Benzmüller C, Stuckenschmidt H, editors. KI 2019: Advances in Artificial Intelligence. Cham: Springer International Publishing; 2019. p. 182–187.
51. Mnih V, Kavukcuoglu K, Silver D, Graves A, Antonoglou I, Wierstra D, et al. Playing atari with deep reinforcement learning. arXiv preprint arXiv:13125602. 2013;;
52. Schulman J, Wolski F, Dhariwal P, Radford A, Klimov O. Proximal policy optimization algorithms. arXiv preprint arXiv:170706347. 2017;;
53. Tieleman T, Hinton G. Lecture 6.5-rmsprop: Divide the gradient by a running average of its recent magnitude. COURSERA: Neural networks for machine learning. 2012;4(2):26–31.
54. Cuccu G, Togelius J, Cudré-Mauroux P. Playing atari with six neurons. arXiv preprint arXiv:1806.01363. 2018;;
55. Savinov N, Dosovitskiy A, Koltun V. Semi-parametric topological memory for navigation. arXiv preprint arXiv:180300653. 2018;;
56. Liu K, Kurutach T, Tung C, Abbeel P, Tamar A. Hallucinative Topological Memory for Zero-Shot Visual Planning. arXiv preprint arXiv:200212336. 2020;;
57. Ebert F, Finn C, Dasari S, Xie A, Lee A, Levine S. Visual foresight: Model-based deep reinforcement learning for vision-based robotic control. arXiv preprint arXiv:181200568. 2018;;

58. Hamilton W, Fard MM, Pineau J. Efficient learning and planning with compressed predictive states. *The Journal of Machine Learning Research*. 2014;15(1):3395–3439.
59. Cassandra AR. A survey of POMDP applications. Working notes of AAAI 1998 fall symposium on planning with partially observable Markov decision processes; 1998;1724.